In Situ Solution Crystallization Study of *n*-$C_{246}H_{494}$: Self-Poisoning and Morphology of Polymethylene Crystals

Edy G. R. Putra and Goran Ungar*

Department of Engineering Materials, University of Sheffield, Sheffield S1 3JD, U.K.

Received January 22, 2003; Revised Manuscript Received April 28, 2003

ABSTRACT: An in situ study of solution crystallization kinetics and morphology of the long alkane *n*-$C_{246}H_{494}$ has been performed by interference optical microscopy using a *T*-jump hot stage. The crystallization temperatures (T_c) covered the full range of extended-chain and part of the once-folded chain range. A drastic change in crystal habit, from broad curved-faced "truncated lozenge" to needle-shape, occurs as T_c is lowered toward the extended- to folded-chain transition. Crystal shapes were fitted to the Mansfield ellipse and T_c dependencies of the following parameters were determined: growth rates of {100} and {110} faces (G_{100} and G_{110}), as well as the rates of secondary nucleation i_{100} and layer propagation v_{100} on {100} faces. With decreasing T_c, all four rates first pass through a maximum and then a minimum at the transition. G_{100} is more retarded by self-poisoning than G_{110}. Furthermore, at the minimum i_{100} is impeded significantly more compared to v_{100}, resulting in straight {100} facets. The fact that v_{100} passes through a minimum is the first evidence that the barrier to layer propagation ("substrate completion") is entropic rather than surface energy based. Significantly, the changes in crystal habit with decreasing T_c correspond to similar albeit less drastic changes which occur in polyethylene with *increasing* T_c. It is thus suggested that self-poisoning also operates in polyethylene, and increasingly so at higher temperatures. Finally, the binary phase diagram $C_{246}H_{494}$−*n*-octacosane solvent exhibits classical behavior, reasonably well described by the Flory−Huggins theory.

I. Introduction

Crystallization rate *G* of monodisperse normal alkanes with 150 to 294 C atoms has been shown to display unusual temperature and concentration behaviors. As supercooling (ΔT) of the melt[1] or solution[2] increases from zero, the crystal growth rate increases at first but then reaches a maximum followed by a pronounced minimum, beyond which *G* increases again steeply. Above the temperature of the minimum, crystals grow with extended chains, while below it they grow either with once-folded chains (solution crystallization) or in the noninteger form (melt crystallization). In the latter form, some chains are once-folded and others are not, traversing the crystal layer only once and remaining half-amorphous.[3] The minimum occurs both in the case of crystal growth and primary nucleation.[4] The $G(\Delta T)$ minimum has also been observed at the transition between the once-folded and twice-folded chain crystallization regimes.[5,6]

Recently, equivalent anomalous behavior of *G* has been observed as a function of concentration.[7] With increasing supersaturation $(c - c_0)/c_0$ (c_0 is the concentration of saturated solution), *G* of extended-chain crystals increases at first but then reaches a maximum. Beyond the maximum the growth rate *G* decreases with increasing concentration until a minimum is reached. After this $G(c)$ increases again, now being the growth rate of once-folded chain crystals. The negative gradient dG/dc can be rather steep; i.e., the reaction order *n* becomes strongly negative, reaching values as low as −5 to −6. The acceleration of crystal growth on dilution causes another intriguing phenomenon termed "dilution wave", observed experimentally[7] and interpreted theoretically in terms of a reaction diffusion equation.[8]

The retardation in crystallization of extended chains, both with increasing supercooling and increasing supersaturation, has been attributed to the same phenomenon of surface "self-poisoning",[1] whereby temporary depositions of folded chains block the productive attachment of extended chains. The classical "coarse-grain" nucleation theory of polymer crystallization has not been able to reproduce the observed anomalies adequately. In contrast, application of the simplest of the "fine-grain" models, where the attachment and detachment of a full stem (extended chain) is broken up into two consecutive steps (two half-stems),[9] gave a good semiquantitative match with the overall shape of both the experimentally observed $G(T)$ and $G(c)$. In the latter model the experimentally verified rule[10] was applied that extended chains cannot deposit onto folded chains, while the reverse is allowed. The factor in the expression for *G* which is responsible for the anomalous retardation is $(1 - A/B)$, where *A* and *B* are the attachment and detachment rates of the first half-stem (or folded chain). The B/A ratio represents the blocked fraction of the surface, and as $B/A \rightarrow 1$, $G \rightarrow 0$ at the minimum. In the case of $G(T)$ this happens as *B* slows down on approaching the folded-chain melting point from above. In the case of $G(c)$, the minimum occurs as, with increasing concentration, *A* increases to match *B*.[7]

In this paper we report the results of an in situ optical microscopy study of solution crystallization of long alkane $C_{246}H_{494}$. We measure the growth of crystals directly and also analyze the crystal habits. Consequently, these experiments provide separate information on the growth rate of {110} and {100} faces, G_{110} and G_{100}. Through the analysis of curvature of the {100} faces, the experiments also allow separate determination of the initiation rate (*i*) and propagation rate (*v*) of new layers of stems; hence, the effect of self-poisoning

10.1021/ma034074h CCC: $25.00
Published on Web 06/18/2003

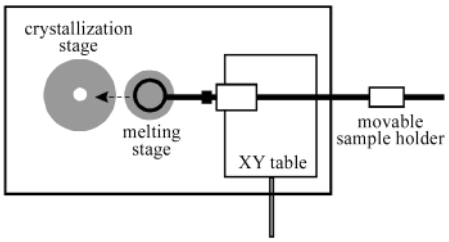

Figure 1. Schematic diagram of the *T*-jump microscopy cell used in the crystallization experiments.

on each of these two rates is established separately. As a result, new conclusions are drawn on the detailed nature of self-poisoning and on its relevance to crystallization of ordinary polydisperse polymers. Preliminary results of a more comprehensive study of solution crystallization kinetics of four long alkanes, from $C_{162}H_{326}$ to $C_{294}H_{590}$, have been summarized recently.[11]

II. Experimental Section

Long-chain *n*-alkanes $C_{162}H_{326}$ and $C_{246}H_{494}$, used in this work, were kindly provided by Dr. G. M. Brooke of the University of Durham, U.K.[12] The solvent used was octacosane (*n*-$C_{28}H_{58}$) from Sigma-Aldrich. Particular care was taken to obtain and maintain solution homogeneity by quench-freezing the solution before storage, placing a solid sample on a coverslip, heating to above the dissolution temperature, and covering with a preheated second coverslip before cooling. Transmission interference contrast microscopy was employed using an Olympus BX 50 microscope equipped with a custom-designed *T*-jump cell manufactured for us by Linkam. The cell contains two silver heating stages and a mechanism for rapid sample transfer from the melting to the crystallization stage. The stage is schematically drawn in Figure 1.

Image sequences were recorded using either a video camera−frame grabber system or a digital camera with a cooled chip.

The experiments were designed to allow rapid attainment of crystallization temperature T_c. Thus, the solution was kept between small (6 mm diameter) coverslips of 0.1 mm thickness. The temperature vs time profiles were determined for different *T*-jumps using the linear growth rate of crystals of pure long paraffin from the melt. The time for the growth rate to attain a constant value was taken as the time for temperature equilibration of the sample between the coverslips. Figure 2 shows one example of such calibration using the alkane $C_{162}H_{326}$. From the crystal length vs time curve (Figure 2a) it can be seen that the asymptotic slope was reached 2 s after the sample had been moved to the crystallization stage. From the derivative of the size/time curve, the growth rate $G(t)$ is obtained. Having also determined the temperature dependence of the linear growth rate of $C_{162}H_{326}$, the temperature vs time profile $T(t)$ of the specimen between the coverslips could be derived—see, e.g., Figure 2b. We found that having the means to effect a rapid temperature jump with no overshoot and a known and nearly rectangular temperature−time profile is indispensable for obtaining trustworthy results, particularly in experiments with alkanes shorter than $C_{246}H_{494}$ and in melt-crystallization work where the $dG/d(\Delta T)$ gradient is steep.

In certain cases, after completing the crystallization experiment, octacosane solvent was replaced by toluene which was then evaporated, leaving dry crystals for observation with higher contrast and resolution.

III. Results

III.1. Alkane−Solvent Phase Diagram. First the binary phase diagram $C_{246}H_{494}$−octacosane was determined. A series of solutions were prepared in small test tubes, ensuring uniform mixing. Both the equilibrium liquidus curve for extended-chain crystals, $T_d^E(c)$, and the metastable equilibrium liquidus curve for once-folded chain crystals, $T_d^F(c)$, were determined directly under the optical microscope. $T_d^E(c)$ was established by observing the disappearance of the last trace of extended-chain crystals in solution under virtually isothermal conditions. The crystals had previously been grown at low supercooling in order to obtain them as defect-free as possible. Experimental $T_d^E(c)$ values are shown as empty circles in Figure 3. The line represents the closest fit with the Flory−Huggins relation[13]

$$\left(\frac{1}{T_d}-\frac{1}{T_m^\circ}\right)=\left(\frac{R}{\Delta H_u}\right)\left(\frac{V_u}{V_1}\right)\left[\left(1-\frac{1}{h}\right)v_1-\chi_1 v_1^{\,2}-\frac{\ln v_2}{h}\right]$$

where T_d is the final dissolution temperature of the long alkane, T_m° is its melting temperature, ΔH_u the heat of fusion per its repeating unit (4.10 kJ/mol), V_u and V_1 are, respectively, the molar volumes of the long alkane

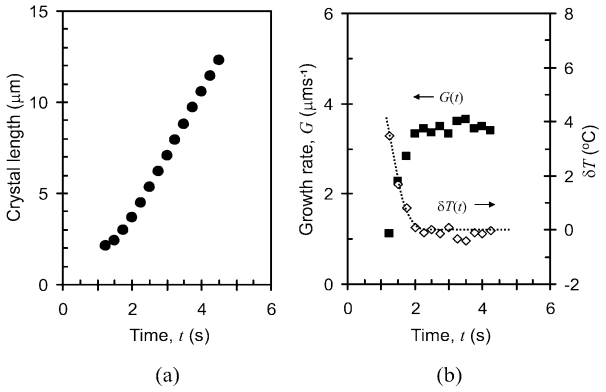

Figure 2. Determination of the temperature−time profile of the specimen between coverslips after the temperature jump using the cell in Figure 1. (a) Crystal length vs time of a crystal of $C_{162}H_{326}$ growing from the melt; time is counted from the instant of the arrival of the coverslip−sample sandwich onto the crystallization stage preset at T_c. (b) Time dependence of the crystal growth rate (derivative of (a)) and of the temperature difference, $\delta T = T_s - T_{cs}$, between the sample, T_s, and the crystallization stage, T_{cs}, calculated therefrom, applying the known linear dependence of the growth rate on supercooling.

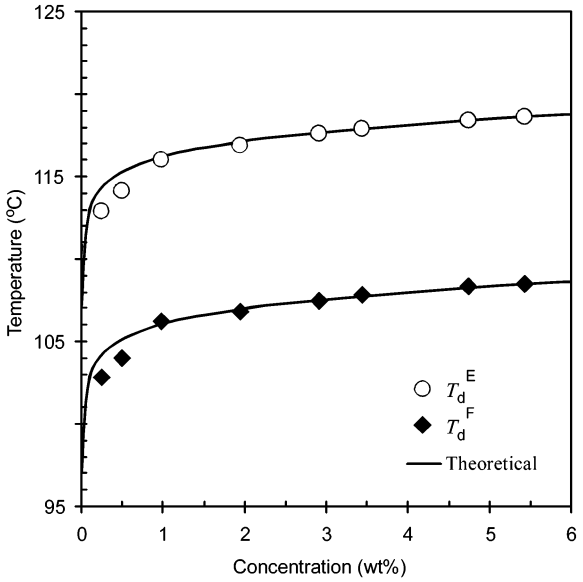

Figure 3. Concentration dependence of final dissolution temperature of extended-chain (empty circles) and once-folded chain crystals (solid diamonds) of $C_{246}H_{494}$ in octacosane. Solid lines represent the best fit Flory−Huggins function.

repeat unit (CH_2) and that of the diluent (octacosane) molecule ($V_u = 14$ cm^3/mol, $V_1 = 509$ cm^3/mol), and χ_1 is the Flory−Huggins interaction parameter with a best fit value of $\chi_1 = 0.15$. v_1 and v_2 are volume fractions of the diluent and the long alkane, and h is the number of repeat units per molecule. The experimental melting point of pure extended-chain $C_{246}H_{494}$, $T_m^E = 128.6$ °C, was taken as $T_m°$ for the equilibrium liquidus.

Experimental values for dissolution temperatures of once-folded chain crystals, $T_d^F(c)$, are obtained by direct observation of the disappearance of such crystals. As will be shown further below, folded and extended-chain crystals can be easily distinguished by their appearance and their growth rates. Strictly isothermal measurements of $T_d^F(c)$ were not possible due to the transformation of folded-chain into extended-chain crystals at that temperature. Thus, a series of measurements were carried out at different heating rates (5−20 K/min) and the obtained dissolution temperatures were extrapolated linearly to zero heating rate. Experimental $T_d^F(c)$ points are shown in Figure 3 as solid diamonds, and the connecting line is the best fit to the Flory−Huggins theory, using the same χ parameter as for $T_d^E(c)$ above, but with a melting point value $T_m^F = 118.6$ °C. Thus, the two liquidus curves run parallel to each other, with an offset of $T_d^E(c) - T_d^F(c) = T_m^E - T_m^F = 10.1$ K. This temperature offset, which is mainly due to the work of chain folding,[14,15] should be compared with the measured melting point difference $T_m^E - T_m^F$ of 7.0 K.[16] The additional 3.1 °C suppression of T_d^F relative to T_d^E is attributed, at least partly, to crystal imperfections caused by the lack of annealing of solution-grown folded-chain crystals.

The phase diagram in Figure 3 is at odds with the reported results on dissolution temperatures of long alkanes in toluene determined by DSC.[17] There it was claimed that alkanes above and including $C_{198}H_{398}$ exhibit "polymer-type" behavior, i.e., that T_d remains constant as $c \to 0$. While there may be differences due to the different solvent, we believe that the more likely cause is the difference in the methods used for determination of T_d. In the case of T_d^E, our method is an equilibrium one; i.e., zero heating rate is used. Furthermore, the phase diagram for $C_{198}H_{398}$ and a different solvent, phenyldecane, was found to be similar to the present one.[7]

III.2. Growth Rates and Crystal Habits. Figure 4 shows a typical example of time dependence of crystal dimensions parallel to the a axis (width) and b axis (length) during the growth of a $C_{246}H_{494}$ crystal from solution. To obtain the growth rate for the initial concentration (4.75% in this case), the slope of $d/2$ vs time was extrapolated to $d = 0$, where d is the dimension of the crystal in the appropriate direction.

Figure 5 shows the temperature dependence of growth rates normal to {110} and {100} planes, respectively, for $C_{246}H_{494}$ crystallizing from a 4.75% solution in octacosane. Typical crystal habits for selected temperatures (T_c), indicated on the $G(T)$ curves, are also shown. In the entire T_c region covered by Figure 5, crystals are of the truncated lozenge type (type B crystal[18]). This habit, with four {110} and two more or less curved {100} faces, is particularly clear in the $T_c = 116.3$ °C micrograph and in the two micrographs of folded-chain crystals at 107.7 °C and 105.7 °C (cf. also Figure 9). With temperature decreasing from $T_c = 116.3$ °C, {110} faces decrease in length relative to {100} faces, and the

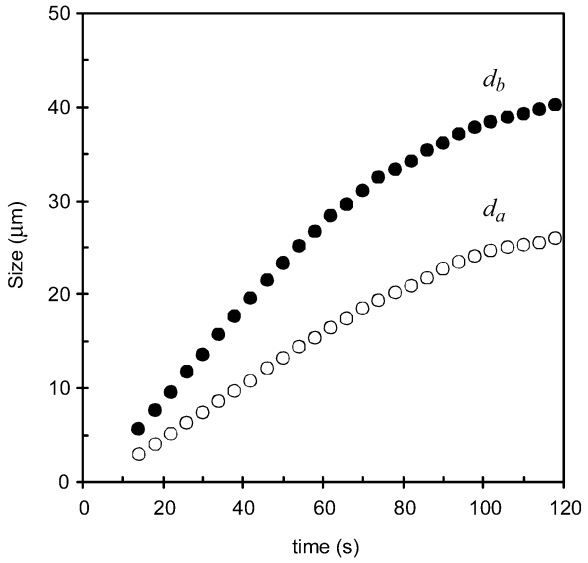

Figure 4. Example of size d vs time functions for a growing crystal of $C_{246}H_{494}$. Initial concentration 4.75% in octacosane, $T_c = 115.2$ °C. Time is counted from the moment the specimen temperature reached T_c. d_a and d_b are dimensions along the crystal a and b axis, respectively.

crystals become more leaf-shaped. At first the curvature of the {100} faces increases somewhat and then, with further undercooling, it decreases, resulting in flat {100} facets in the needlelike crystals at the growth rate minimum (see further below). The growth rate $G_{100} = G_a$ was determined from the width of the crystal d_a. G_{110} was determined as $G_{110} = G_b/\sin\gamma$, where G_b is the growth rate along the long axis, and $\gamma = \arctan(a_0/b_0)$, a_0 and b_0 being the unit cell parameters. {110} edges are observed in the crystals at most temperatures, but even where they are not clearly resolved, type A crystal habits[18] are not observed. Type A crystals are common in melt crystallization and have tapered acute ends with straight edges tangential to the elliptical portions of {100} faces. In the absence of such habits, even where {110} faces are not clearly discerned, $G_{110} \cong G_b/\sin\gamma$.

As a function of T_c both G_{100} and G_{110} rates show a maximum and then a minimum close to the dissolution temperature of folded-chain crystals T_d^F. Previous direct rate measurements were, as a rule, done for crystal growth from melt and yielded G_b.[19,20] As mentioned above, G_b may or may not be directly related to G_{110}. First direct growth rate measurements from solution were reported for a long alkane only recently.[7] Here we find from Figure 5 that the maximum in G_{100} is located at a higher temperature than the maximum in G_{110}. Compared to {110} growth, {100} growth becomes retarded already at a smaller supercooling, further away from T_d^F.

The temperature of the growth rate minimum, as defined by $G_j^{\text{extended}} = G_j^{\text{folded}}$, is 0.4 °C lower for {110} growth ($j = 110$) as compared to that for {100} growth ($j = 100$). Compared to the {110} minimum, the {100} minimum is far deeper, the growth virtually coming to a halt. The temperature of the minimum in overall crystallization rate is thus defined by the {100} minimum. Note that three different extended-to-folded growth transition temperatures, related to three different growth face types, were observed in fractionated poly(ethylene oxide);[10] however, G did not pass through a minimum.

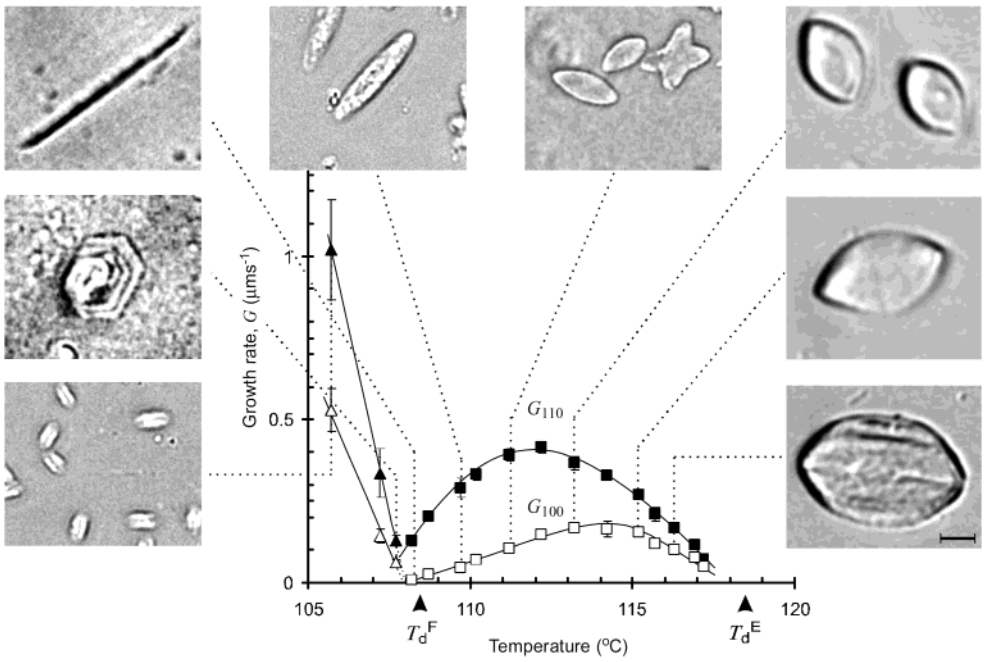

Figure 5. Initial rates of growth of $C_{246}H_{494}$ crystals normal to {110} and {100} planes, G_{110} and G_{100}, vs crystallization temperature from an initially 4.75% solution in octacosane. The associated interference optical micrographs show typical crystal habits recorded in situ during growth from solution at selected temperatures. The experimental G values are averages over many crystals. Standard deviation is represented by error bars or the symbol size. Scale bar in the micrograph represents 10 μm.

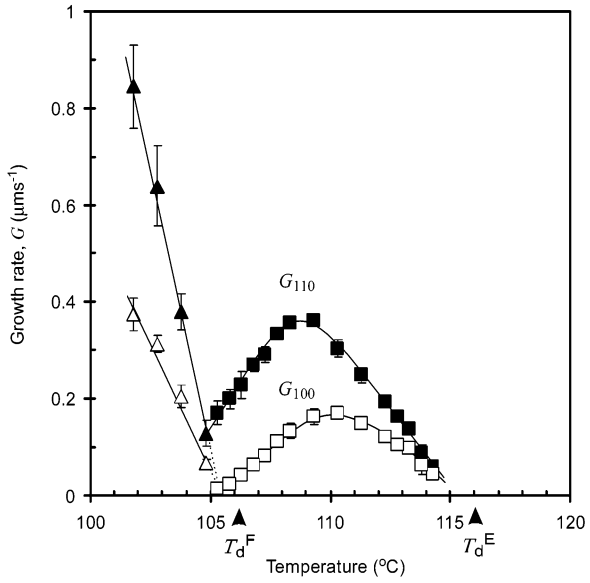

Figure 6. Initial rates of growth of $C_{246}H_{494}$ crystals normal to {110} and {100} planes, G_{110} and G_{100}, vs crystallization temperature from an initially 0.98% solution in octacosane.

Figure 6 shows the dependence of G_{100} and G_{110} on crystallization temperature for the lower solution concentration of 0.98%. The corresponding crystal habits are displayed in Figure 7. Compared to the diagram for $c = 4.75\%$ in Figure 5, all curves in Figure 6 are shifted to lower temperatures by ca. 3 K, in accord with the phase diagram in Figure 3. In other respects, the shapes of the two growth rate curves are rather similar in the two diagrams. Note that the maximum values for $G_{100}^{\text{extended}}$ and $G_{110}^{\text{extended}}$ are almost exactly the same, despite an almost 5-fold difference in concentration. This has already been noted in the case of $C_{198}H_{398}$.[7] It is the result of cancellation of two opposing concentration-dependent effects: increasing attachment rates of extended chains and increasing attachment rates of the blocking folded chains.

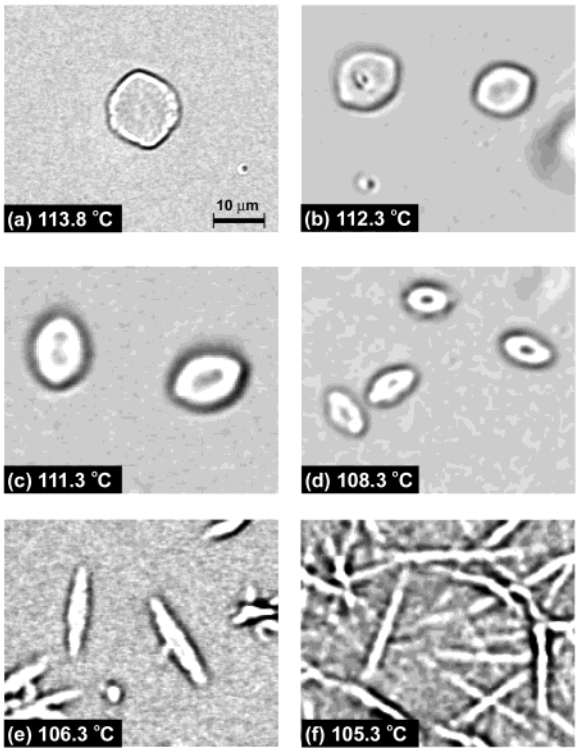

Figure 7. Interference optical micrographs of $C_{246}H_{494}$ crystals recorded during growth from an initially 0.98% solution at the temperatures indicated.

The ratio G_{110}/G_{100} is plotted against crystallization temperature in Figure 8 for both 0.98% and 4.75% concentrations. One should remember that the rates are obtained by extrapolation to zero size, i.e., to the conditions of initial solution, and thus the aspect ratios of the crystals shown in the micrographs are not

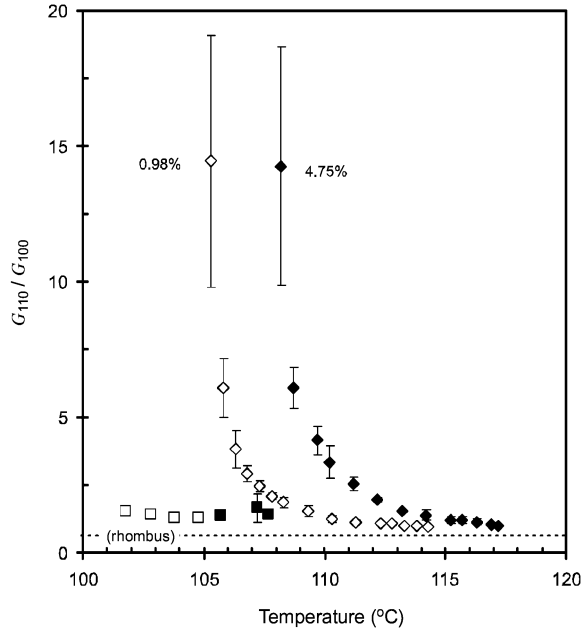

Figure 8. G_{110}/G_{100} ratio vs crystallization temperature for c = 4.75% (full symbols) and c = 0.98% (open symbols). Key: diamonds, extended chains; squares, once-folded chains. The horizontal line marks the G_{110}/G_{100} value for nontruncated faceted lozenges.

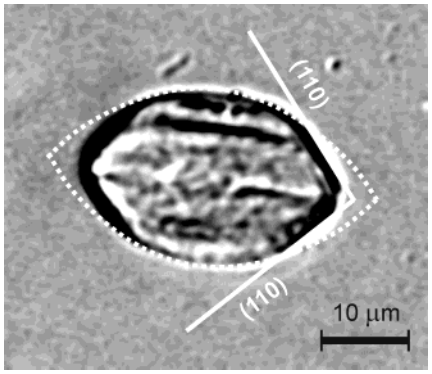

Figure 9. Example of fitting a corrected Mansfield ellipse (eq 1a,b, white dotted line) to {100} faces of a $C_{246}H_{494}$ crystal (T_c = 116.3 °C, 4.75% initial concentration). $ib_o^2/2v = 0.31$. The solid white lines are extrapolations of the {110} faces.

necessarily an accurate reference for obtaining the values of G_{110}/G_{100}. At low supercooling, far above the temperature of the growth minimum, the G_{110}/G_{100} value is not much higher than the limiting ratio for rhombic lozenge-shape crystals (horizontal line in Figure 8). However, with increasing supercooling the ratio increases progressively and diverges at the rate minimum due to the disproportionate suppression of growth on the {100} faces. Below the temperature of the minimum the G_{110}/G_{100} ratio typical of low supercooling is reestablished and the cycle begins to repeat itself, this time with folded-chain growth.

III.3. Rates of Step Initiation (*i*) and Step Propagation (*v*). The rates of initiation i and propagation v of new layers of chains on {100} faces were obtained by fitting the curvature of these faces to the Mansfield ellipse[21]

$$\left(\frac{x_p}{v}\right)^2 + \left(\frac{y}{\frac{a_0}{2}\sqrt{2iv}}\right)^2 = 1 \qquad (1a)$$

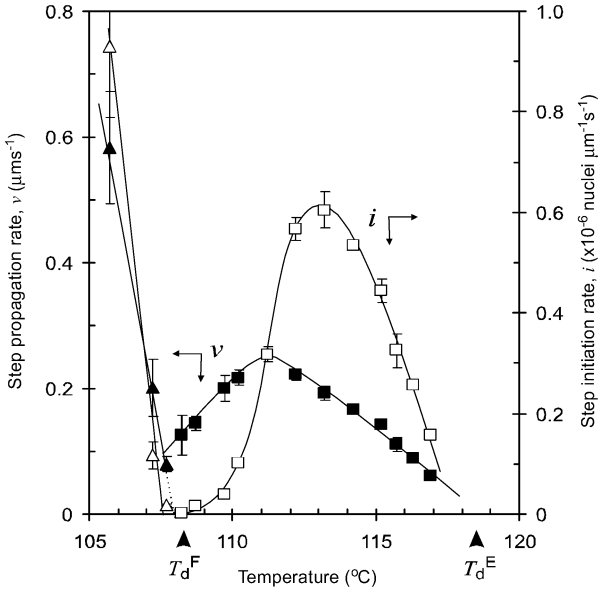

Figure 10. Step initiation rate i (empty symbols) and step propagation rate v (full symbols) on the {100} faces as a function of crystallization temperature for $C_{246}H_{494}$ crystals growing from 4.75% octacosane solution. Key: squares, extended chain; triangles, folded chain growth.

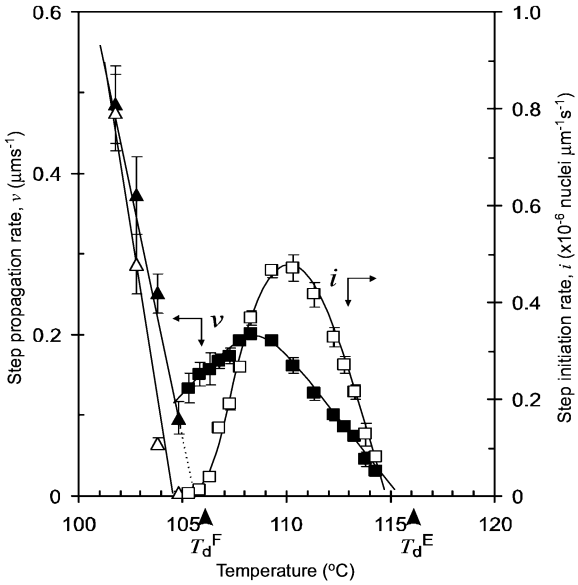

Figure 11. Step initiation rate i and step propagation rate v on the {100} faces as a function of crystallization temperature for $C_{246}H_{494}$ crystals growing from 0.98% octacosane solution. Symbols are as in Figure 10.

where x_p for the primitive rectangular lattice was converted to x for the effectively centered lattice appropriate to crystals of alkanes or polyethylene via[18]

$$x = x_p + \left(\frac{a_0}{2}\sqrt{2iv} - y\right)\cot\gamma \qquad (1b)$$

Equation 1a was scaled with $y_{x=0} = G_{100}$. Figure 9 shows an example fit of an extended-chain crystal with highly curved {100} faces (T_c = 115.2 °C from 4.75% solution).

The resulting secondary nucleation rate i (the rate of initiation of steps) and the step propagation rate v (or "substrate completion" rate) are plotted against T_c in Figure 10 for the 4.75% solution and Figure 11 for the 0.98% solution.

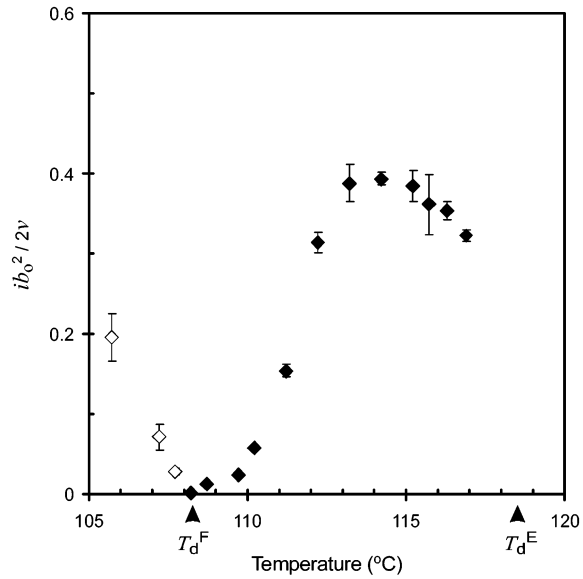

Figure 12. Initiation to propagation rate ratio $ib_o^2/2v$ against T_c for $C_{246}H_{494}$ crystal growth from a 4.75% octacosane solution.

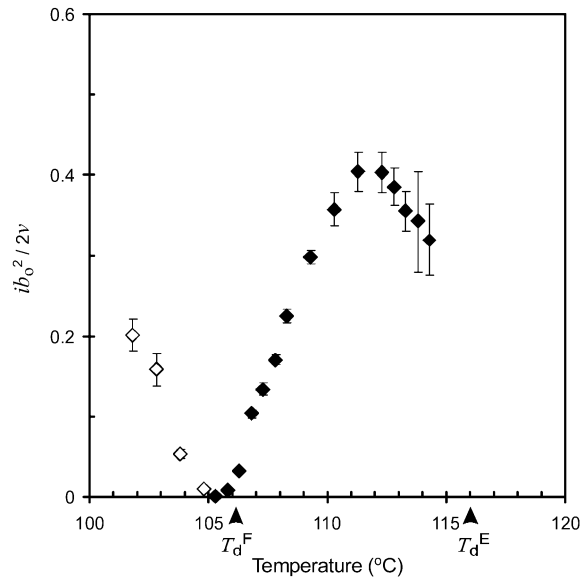

Figure 13. Initiation to propagation rate ratio $ib_o^2/2v$ against T_c for $C_{246}H_{494}$ crystal growth from a 0.98% octacosane solution.

Figures 10 and 11 show that both i and v display a maximum and a minimum as a function of ΔT. However, the retardation in layer initiation is far more pronounced than that in layer propagation. While v drops to half its maximum extended-chain value at the minimum, i is reduced to only 1/500 of its value at the maximum. Furthermore, $di/d(\Delta T)$ becomes negative as far as 5.0 K above the temperature of the minimum, compared to only 3.0 K for $dv/d(\Delta T)$. The equivalent values for 0.98% solution are the same (5.0 and 3.0 K, respectively). This disproportionately large retardation in i beyond a certain ΔT causes increasing elongation of the Mansfield ellipse, so that near the growth minimum {100} faces become virtually flat. This leads to narrow ribbon-shaped habits (see Figure 5, 108.2 °C), with an aspect ratio of the order of 15, the length of the ribbons being limited only by the less retarded G_{110}.

It is informative to observe temperature dependence of the initiation/propagation ratio. Figures 12 and 13 show $ib_o^2/2v$ against crystallization temperature. This parameter gives the ratio $p_\uparrow/p_\leftrightarrow$ of probabilities of deposition of a stem as a secondary nucleus against the probability of its attachment to a niche on either side of a spreading layer. The $ib_o^2/2v$ ratio is seen to depend strongly on temperature. Within the extended-chain growth range it has a maximum, decreasing toward both the low-temperature and the high-temperature ends of the range. In the folded-chain growth regime the trend seems to begin to repeat itself, but unfortunately, only the top of the folded-chain T_c range was accessible to reliable measurement.

IV. Discussion

This first account of the effect of self-poisoning on crystal habits shows an unusual variation in form within a comparatively narrow interval of crystallization temperatures. Less pronounced changes have been observed in melt-crystallization of sharp fractions of poly(ethylene oxide),[10,22] but some spectacular morphologies resulting from crystal thickening ("pathological" crystals) were recorded in a very narrow transition range.[10]

The present examination of crystal habits has uncovered a number of new features of the self-poisoning effect. Crystal shapes have been analyzed here in terms of (1) the separate rates of initiation (i) and propagation (v) of steps on the {100} face and (2) the ratio of growth rates G_{110}/G_{100}. The behavior of i and v and its implications are discussed in section IV.1. The behavior of G_{110} vs G_{100} is discussed in section IV.2. The conclusions are extrapolated to polymers in section IV.3.

IV.1. Effect of Self-Poisoning on *i* and *v*. IV.1.A. *i* and *v* for $T_c \geq T_{max}$. The T_c range between the extended-chain dissolution temperature T_d^E and the temperature of the growth rate maximum (T_{max}) is discussed first (T_{max} is dependent on the rate parameter in question). Referring to Figure 12 and Figure 13, it is not surprising to find that the i/v ratio decreases as T_d^E is approached from below. Nucleation generally requires larger supercooling compared with growth, due to the larger energy barrier for nucleation. As is well-known, the critical nucleus size increases with decreasing supercooling ΔT. For nucleation-controlled growth, if crystals could be grown within reasonable time at sufficiently small ΔT, any growth face would be flat and regime I conditions would apply (here we neglect the possible limitation of "substrate length" L_p due to, e.g., crystal defects). However, in the present case of $C_{246}H_{494}$ crystallizing from octacosane, the range where such conditions apply, if existing at all, is very narrow and even at only 1 K supercooling the growth face is already curved. Nevertheless, there is a clear trend of decreasing i/v (decreasing curvature) as $\Delta T \rightarrow 0$ in the case of both 0.98% and 4.75% solutions, particularly below T_d^F. This suggest that the growth is a nucleated process, even if the nucleation and propagation rates are not markedly different. Had the curvature been due to the roughening transition,[23] it would have, if anything, increased with T_c.

In contrast to the behavior of alkane $C_{246}H_{494}$, the trend of decreasing i/v and reducing growth face curvature as $\Delta T \rightarrow 0$ has not been reported in polyethylene crystallized from solution at high temperatures. This may be due to the complicating fact that in a polymer, as $\Delta T \rightarrow 0$, lamellar thickness increases at the same time, hence the pure effect of temperature cannot be

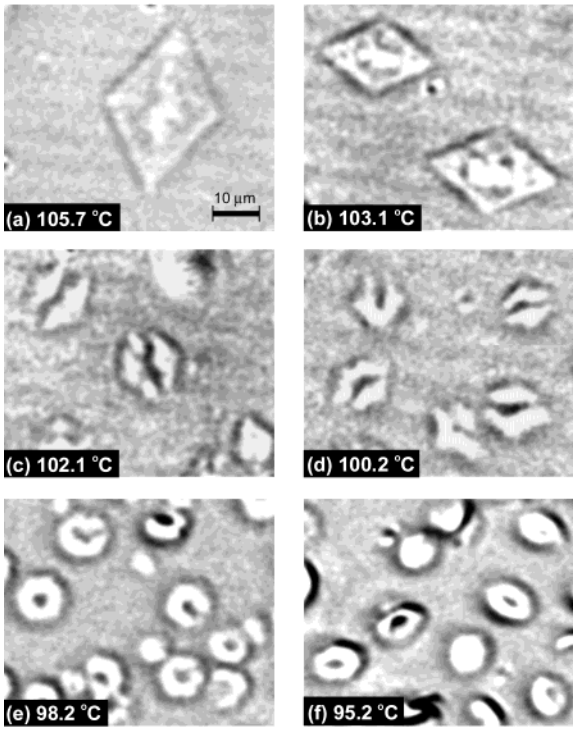

Figure 14. Interference optical micrographs of single crystals of alkane $C_{162}H_{326}$ grown from an initially 1.02% solution in octacosane at the temperatures indicated.

isolated. Separation of the effects of crystallization temperature and lamellar thickness is indeed one of the main advantages of studying monodisperse oligomers, as detailed in a recent review.[24]

The work by Mansfield,[21] Point and Villers,[25] and Toda,[18] based on the groundwork by Frank,[26] has shown that the cause of curved lateral crystal faces is a low value of v. A low value of v could, in principle, arise from a number of obstructing conditions. Hoffman and Miller suggested that the obstruction is due to mounting strain caused by chain folds,[27] while Toda attributed it to impurities.[28] However, in several aspects, the present results point strongly to self-poisoning as the cause of slow step propagation and hence curved lateral faces. The evidence is discussed further below. Confining the current argument to the $T_{max} < T_c < T_d^E$ range, we first make a comparison between crystal morphologies of the presently studied alkane $C_{246}H_{494}$ and the previously investigated $C_{162}H_{326}$.[29]

For $C_{162}H_{326}$ there is less evidence of growth obstruction at low supercooling. Thus, $C_{162}H_{326}$ develops faceted rhombic crystals from octacosane solution close to the extended chain dissolution temperature T_d^E—see Figure 14a,b.[29] Under those circumstances G_{100} is too fast, i.e., too weakly retarded, for {100} faces to be observed, a fact significant in its own right. Although at low ΔT the curvatures of {100} crystal faces cannot be compared for the two alkanes, the curvatures of {110} faces can. Comparing {110} faces of crystals of $C_{162}H_{326}$ (Figure 14a-d) and $C_{246}H_{494}$ (Figure 5a and Figure 7a), the latter show evidence of curvature while the former do not. The above observations imply that, at low supercooling, both G_{100} relative to G_{110}, and v relative to i, are less retarded in $C_{162}H_{326}$ than they are in $C_{246}H_{494}$. To understand this difference between the two alkanes we note that, near its T_d^E, $C_{246}H_{494}$ is closer to its T_d^F ($T_d^E - T_d^F$ = 10.1 K) as compared to $C_{162}H_{326}$ ($T_d^E - T_d^F$ = 16.4 K). Incidentally, the difference $T_d^E - T_d^F$ is inversely proportional to chain length L, according to the simple Hoffman–Weeks relationship[30] (σ_e = fold-surface free energy, S_d = entropy of dissolution):

$$T_d^E - T_d^F = \frac{2\sigma_e}{L\Delta S_d}$$

As a consequence of the larger $T_d^E - T_d^F$ for $C_{162}H_{326}$, the attachment/detachment rate ratio A/B for folded chains close to T_d^E is low and the free (nonblocked) fraction of the surface $1 - A/B$ is not appreciably lower than 1 (see Introduction). For $C_{246}H_{494}$, in contrast, the smaller $T_d^E - T_d^F$ means that even if T_c is close to T_d^E, $1 - A/B$ is already significantly lower than 1; hence, the growth is retarded.

At its maximum, the ratio of probabilities of a stem forming a secondary nucleus and of its attaching at a *niche*, $p_\uparrow/p_\leftrightarrow = ib_0^2/2v$, approaches $^1/_2$. The value of $^1/_2$ is most likely an overestimate since the theory cannot be applied properly for such a high $p_\uparrow/p_\leftrightarrow$ ratio.[21] Nevertheless, the value of $^1/_2$ means that the growth ceases to be a nucleated process. Thus, the rough-surface growth mode[23] appears to be approached in solution crystallization of extended-chain alkane $C_{246}H_{494}$ at small to moderate supercooling. The growth face is highly curved but not yet circular (Figure 9).

IV.1.B. i and v in the Range $T_{min} < T_c < T_{max}$. The aspect ratio of $C_{246}H_{494}$ crystals increases drastically as T_c is lowered from that of the growth rate maximum ($d_b/d_a \cong 2$) to that of the minimum ($d_b/d_a \cong 15$). The aspect ratio of a truncated lozenge crystal is determined by the G_{110}/G_{100} ratio. However, for crystals with curved {100} faces not to turn into leaf-shaped (type A[18]) as G_{110}/G_{100} increases, the step propagation rate v on the {100} faces must keep up with the relative increase in G_{110}. This means that the ratio i/v on the {100} faces must decrease, which is indeed the case for $C_{246}H_{494}$ with T_c decreasing from T_{max} to T_{min} (Figures 10 and 11). In other words, the Mansfield ellipse, which describes the crystal habit bounded solely by {100} faces, must become elongated if the {110} faces are not to grow out. This elongation of the ellipse is clearly seen in Figure 5 and Figure 7. In contrast to the present case, the decrease in i_{100}/v_{100} does not always match the decreases in G_{100}/G_{110}. Thus, in melt-crystallization of long alkanes we commonly observe a change from truncated lozenge (type B) to lenticular (type A) habit with changing T_c.[31] Type A crystals are also common in melt-crystallized polyethylene.[18]

Figures 10 and 11 show that both i_{100} and v_{100} are retarded by self-poisoning and pass through a minimum near T_d^F. However, taking the rates at the maximum as reference, it is clear that step nucleation (i) becomes substantially more retarded than step propagation (v). This is reiterated in Figures 12 and 13 where the $ib_o^2/2v$ ratio is seen to drop to an extremely low value of 1.2×10^{-3} at the rate minimum.

A low i/v value means straight lateral faces and regime I crystallization. Strictly, regime I is obeyed when the Lauritzen parameter $iL_p^2/2v \leq 0.01$, where L_p is the persistence length between surface defects limiting the spread of the layer.[32] As L_p can reasonably be expected to be well above $3b_0$ $\{[(1 \times 10^{-2})/(1.2 \times 10^{-3})]^{1/2} \cong 3\}$, conditions for regime I are not fully met, and we may neglect the effect of limited substrate length L_p.

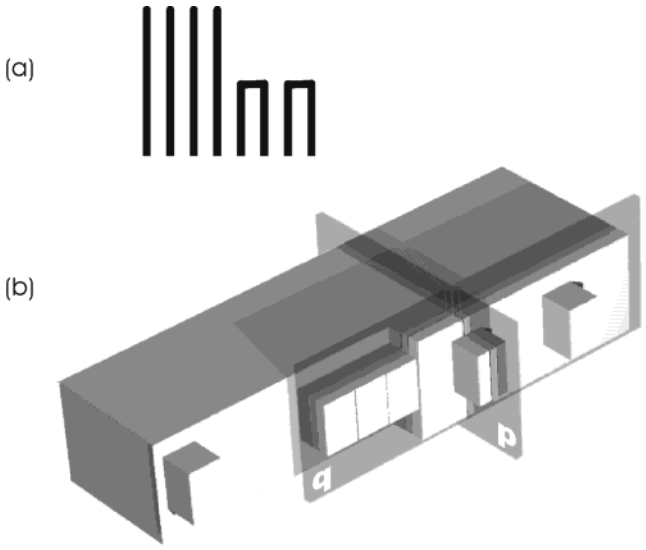

Figure 15. (a) Row of extended chains whose spreading to the right is blocked by deposited folded chains; (b) Schematic view of the growth face of an extended-chain lamellar crystal poisoned by stems of half the chain length. The row-of-stems model can be applied with the row perpendicular to the growth face, as in the previous "rough growth" models[7,9,23] to describe retardation of i (row p), or parallel to the growth face to describe retardation of v (row q).

It may seem paradoxical that *faceted* crystals should appear under conditions where growth is most strongly obstructed. However, faceting is here not due to the ease of substrate completion (high v), but rather to the extreme difficulty of forming a secondary nucleus. That is, not far above the folded chain dissolution temperature, the deposition of an extended chain on a flat surface is disproportionately highly retarded compared to the deposition in an existing *niche*.

In previous analytical and simulation descriptions of the growth rate minimum[7,8] the one-dimensional row-of-stems model was used, the row being normal to the growth face as in Figure 15a. The model is based on that used by Sadler in treating the nonnucleated roughness-pinning growth.[23] The half-stems on the right of the row in Figure 15a represent the blocking folded chains at the crystal surface. However, as the current work shows, the growth is in fact nucleation controlled to a significant degree, implying that obstruction of both initiation and propagation processes should be considered. Figure 15b illustrates this schematically. The two crossed semitransparent planes illustrate how the row model can be applied both normal to the growth face (row p), to describe nucleation, and parallel to the growth face (row q), to describe layer propagation.

Step propagation can be inhibited by folded chains settling in the *niche* at the end of a growing layer (Figure 15b, row q). While this obstruction mechanism may seem obvious, it is not compatible with the classical Lauritzen−Hoffman (LH) nucleation theory of polymer crystallization on two counts. One is the neglect by the theory of depositions of stems shorter than l_{min}, l_{min} being the length of stem whose melting or dissolution temperature is equal to T_c. This neglect is one aspect of the "coarse grain" nature of the LH theory, which has been challenged by Point[33] and Sadler.[23] In the theoretical explanation of the alkane growth rate minimum the coarse-graininess has been circumvented by the simple splitting of extended chains into two equal segments.[8]

IV.1.C. Energy vs Entropy Barrier to Substrate Completion. The second point of disagreement between the classical version of the LH theory and the present finding of a minimum in v concerns the very question of the nature of the free energy barrier for stem deposition. Since v has not been measured previously in alkanes, this issue has not arisen before in connection with the effect of self-poisoning. Figure 16a shows schematically the progress of free energy F of a surface layer with increasing number of deposited extended chains (solid line). Figure 16a is based entirely on surface energy. For each added extended chain, F changes by

$$\Delta F = 2b^2\sigma_e - b^2L\phi_T$$

where b = width of a chain of square cross-section, ϕ_T = bulk free energy of crystallization, and L = extended chain length. For clarity, the diagram is drawn for the case of $\psi = 0$, where ψ is the Lauritzen−Hoffman apportioning parameter. According to the LH theory, the barrier to addition of an extended chain to an existing *niche* is only $2b^2\sigma_e$, and is due to the two added end surfaces; no new side surface is created. This barrier is small (2 kJ/mol) compared with the bulk free energy liberated (26 kJ/mol for $\Delta T = 10$ K), and compared with the barrier $2bL\sigma$ for the deposition of the first chain (75 kJ/mol). More importantly still, the $2b^2\sigma_e$ barrier to deposition of obstructing chains would, if anything, be higher than the barrier for the productive deposition of extended chains. Taking $\sigma_e^{extended} = 0.01$ J m^{-2} and $\sigma_e^{once\ folded} = 0.05$ J m^{-2},[14] the barrier for the obstructing folded depositions would be five times higher (10 kJ/mol) than that for extended chains. Combined with the fact that, for an extended chain, the bulk free energy drop is twice that for a half-chain, there would be no retardation in v due to self-poisoning. Chain-folded attachments would not compete with the extended-chain substrate completion process to any significant extent. While the full line in Figure 16a charts F of extended chain deposition, the dashed lines represent the hypothetical attachments of half-chains to the *niche* at the end of the growing surface layer (note that, for simplicity, the fold energy has been equally split between the first and the second stem of a folded chain).

On the other hand, if it is assumed that the free energy barrier to chain deposition is entropic, and if this assumption is applied to deposition of subsequent as well as the first stem in a layer, then the picture changes drastically and is more adequately represented by Figure 16b. First, the barrier for chain addition must be substantially higher than $2b^2\sigma_e$. In fact under conditions where strongly curved faces can be formed and the $ib_o^2/2v$ ratio reaches $^1/_2$ (see Figures 12 and 13), the barrier for substrate completion must be comparable with that for layer initiation. Second, if the barrier to step propagation is entropic it must depend on the stem length l, as in the case of step initiation. An entropic barrier arises partly from the improbability of stem extension, and is therefore likely to be approximately linear in l and have a form $-TS^* = -kT(\ln \Omega) = -kmT(\ln \omega) \propto l$, where ω is the number of available conformations per segment and m the number of segments in a stem.[34]

If the barrier to deposition of nth stem ($n > 1$) is proportional to l, then the barrier to attachment of half

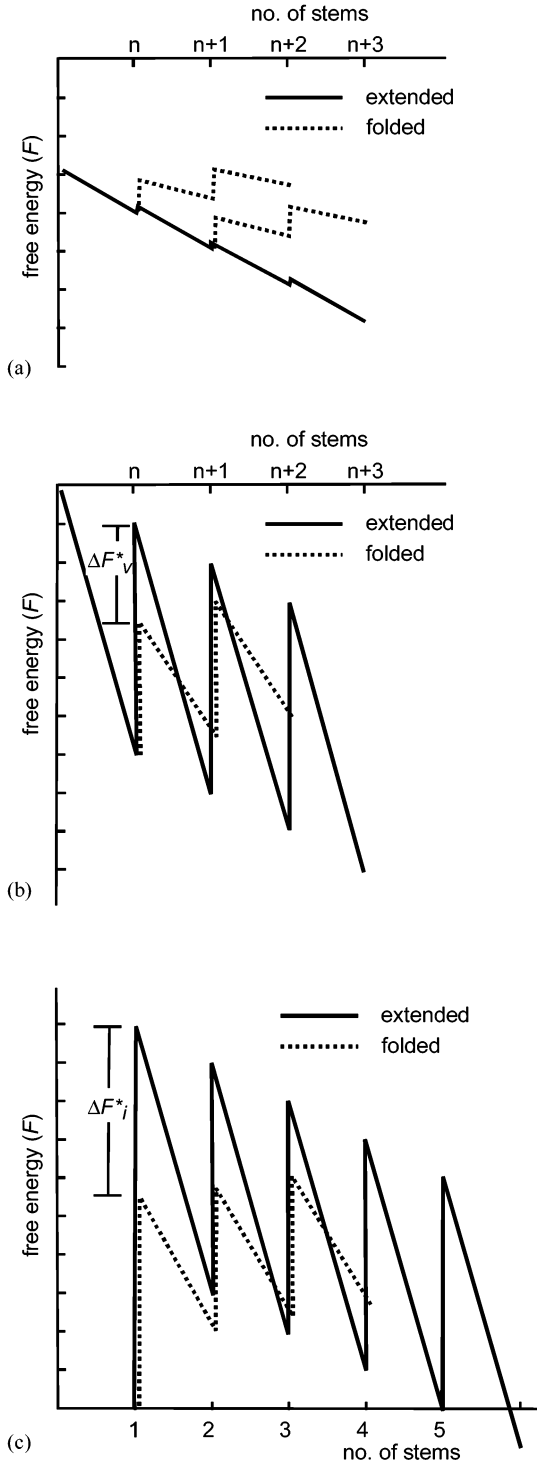

Figure 16. Schematic representation of the progress of free energy of a crystal with increasing number of stems in a layer on the growth face at T_c slightly above T_d^F, i.e., near the growth minimum. Key: solid line, extended-chain deposition; dashed line, obstructing folded-chain depositions. (a) Layer propagation assuming surface energy barrier. (b) Layer propagation assuming the barrier is mainly entropic. (c) Layer initiation and propagation assuming mainly entropic barrier. In parts b and c, diversions along the path of unproductive folded deposition (dashed line) could occur after each extended-chain deposition.

a chain is approximately only half that for attachment of an extended chain, and the deposition rate (A) of the former exceeds that of the latter by the factor $\exp(\Delta F^*_v)$—see Figure 16b. While $L/2$ depositions are unstable above T_d^F, for T_c not far above T_d^F their detachment rate B is low; hence $1 - A/B$, the fraction of time during which the end-of-layer *niche* is blocked, approaches 1 (cf. Introduction). The dashed line in Figure 16b symbolizes the low-barrier blocking process of slightly positive net free energy. The explanation of the reduction in v with increasing supercooling is essentially the same as the previous explanation of the minimum in the overall growth rate, where no distinction was made between initiation and growth of individual layers.

The significance of the presently determined temperature dependence of v is that it provides a direct proof that the free energy barrier to polymer crystal growth is entropic rather than enthalpic. In fact, to our knowledge, this is the first instance where the entropic nature of the barrier has been shown to apply to the process of substrate completion. Previously, the entropic barrier has been considered only in connection with the process of secondary nucleation, i.e., laying down the first stem,[15,33,35] or in the context of the nonnucleated rough-surface growth theory.[23] It may be noted in passing that there exists a difference in the perception of what constitutes the entropic barrier. Point[33] and Hoffman[15] in their different approaches only consider the deposition of one stem at a time, with no regard to interfering attachments; the former by splitting the process into a number of segmental depositions, the latter by relating σ to the characteristic ratio C_∞ of the polymer. The present experimental results show that the blocking (or pinning) chains also have to be included in S^*, in addition to the improbability of stem extension.

Thus, the framework in which the present kinetic and morphological results are best described seems to be a hybrid of the secondary nucleation (LH) theory and the roughness-pinning theory of Sadler. The following features of these theories are incompatible with the present results: LH theory—the coarse grain (one stem = one step) approach and the reliance on surface energy; Sadler's theory—the negation of secondary nucleation.

IV.1.D. Suppression of Secondary Nucleation Rate *i*. As seen in Figures 10−13, retardation of i at the growth rate minimum is far more severe than that of v. Also the gradient $di/d(\Delta T)$ becomes negative at a higher temperature compared to that at which $dv/d(\Delta T)$ turns negative. There are two factors which are expected to contribute to the effect of self-poisoning on i being stronger than that on v. These are discussed below.

(a) The difference ΔF^*_i between barriers to deposition of an extended chain (L stem) and an $L/2$ stem on a flat face is larger (see Figure 16c) than the equivalent difference in the case of deposition into an existing *niche* (ΔF^*_v—Figure 16b). This is because the free energy barrier F^* for deposition of the first stem is higher than that for subsequent stems, both in its energy (E^*) and entropy ($-TS^*$) terms. Regarding the former, there is the additional side surface energy contribution to E^* of nucleation, absent in subsequent *niche* depositions. Regarding the entropic term, $-S^*$ is also higher for the first stem because alignment along a flat face leaves more conformational choices (larger ω) than does alignment along a *niche*. In reality, $-S^*$ is further reduced for a $L/2$ stem by $k(\ln(m/2))$ due to the free choice of longitudinal placement of such a stem on an extended-chain substrate. The result of all these factor will be a ΔF^*_i considerably larger than ΔF^*_v; hence $L/2$ stems will block the deposition of L stems more effectively in the process of initiation than in the process of substrate completion.

(b) The second cause of i being more retarded than v is likely to be the following. Since at low ΔT it takes several extended chains to form a stable new layer, the survival probability of the layer will be further impaired by delays to its growth due to blocking of each successive deposition until the net free energy changes to negative. Thus, even if the first chain had deposited successfully, blocking of the substrate completion process will decrease the survival probability of the layer. While a folded deposition blocks the advance of the layer, it does not correspondingly protect the neighboring extended chain from detachment. The cumulative poisoning of consecutive stages in the growth of a critical secondary nucleus may in fact explain the particularly high temperature at which the retardation in i becomes notable and at which di/d(ΔT) turns negative: although the blocking effect of each individual $L/2$ deposition is small high above T_d^F, at these temperatures it takes more L stems to form a stable layer, making it more vulnerable to self-poisoning.

IV.2. Effect of Self-Poisoning on G_{100} and G_{110}. As seen in Figures 5, 6, and 8, G_{110} is much less retarded at the growth rate minimum than G_{100}. It has been shown above that it is the severe suppression of secondary nucleation (i_{100}) which causes G_{100} to drop to near zero at the minimum. For G_{110}, we do not have separate data on i and v. This is partly because {110} faces are too small in the present crystals for the curvature to be analyzed by optical microscopy, and partly because there is no worked out model for the curvature of {110} faces. As shown recently for the example of $C_{162}H_{326}$, {110} faces are curved asymmetrically since, unlike {100} faces, they do not possess a mirror plane normal to the crystal lamella, hence the layer propagation rates in the right (v_r) and left direction (v_l) are not equal.[29] Incidentally, single crystals with asymmetrically curved {110} faces are also clearly observed in poly(vinylidene fluoride).[36]

It is feasible that, for some reason, i_{110} is considerably less retarded at the {110} growth rate minimum compared to i_{100} at the {100} minimum. However, a possible reason for {110} growth not being retarded drastically may be that {110} growth is not limited by i_{110} at all. Since the length of {110} faces of the needlelike crystals near T_{min} is small, most nuclei on these faces may conceivably be created by spillover from {100} faces at the corner where the two meet. At the present stage, however, this remains a speculation.

IV.3. Relevance to Polyethylene and Polymers in General. Despite the uncertainty as to the cause of weaker retardation in G_{110}, what is clearly evident is that, within a growth branch (extended or once-folded), the trend of change in G_{110}/G_{100} ratio with T_c is exactly opposite of that in polyethylene. This is illustrated in Figure 17, where the G_{110}/G_{100} values for extended-chain $C_{246}H_{494}$ are compared with those obtained from measurements on published micrographs of polyethylene single crystals.[37] While in the alkane the G_{110}/G_{100} ratio increases dramatically with *decreasing* T_c, the lozenge being increasingly truncated, in polyethylene this ratio increases with *increasing* temperature, the rhombic lozenge forming at the lowest temperature and becoming truncated as T_c rises. As already shown, in alkane $C_{162}H_{326}$ crystallized from octacosane, the habit changes from a pure rhombic lozenge at the highest T_c to the highly truncated lozenge closer to the rate minimum (Figure 14).

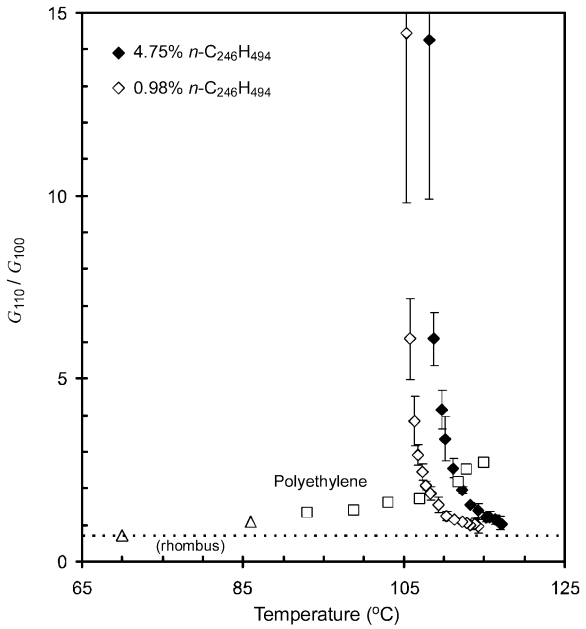

Figure 17. Ratio of growth rates G_{110}/G_{100} vs crystallization temperature for extended-chain crystals of $C_{246}H_{494}$ from 4.75% and 0.98% octacosane solutions and for linear polyethylene from 0.05% (w/v) solutions in short paraffins (□) and xylene (△). The polyethylene crystal at $T_c = 70.0$ °C is a nontruncated lozenge.

Since in alkanes the increase in G_{110}/G_{100} is clearly linked to self-poisoning, we propose that this is also the case for polyethylene. Thus, we suggest that a mechanism closely related to self-poisoning operates also in crystallization of polydisperse polyethylene. We propose further that, by implication, the self-poisoning effect in the polymer is increasingly pronounced at higher T_c. Since in polymers lamellar thickness increases continuously with increasing T_c, one cannot tell whether the increased effect of self-poisoning is a direct effect of temperature or of increasing crystal thickness. Enhanced self-poisoning would thus account, e.g., for the b axis being the primary growth direction in melt crystallized polyethylene, with a axis growth suppressed disproportionately by self-poisoning of {100} faces.

The obstruction of growth faces in polydisperse polymers clearly cannot be described by exactly the same mechanism as in monodisperse alkanes. In polymers a preferred stem length is selected for each temperature from a continuous spectrum, and we cannot talk of "extended chains", "once-folded chains", associated growth transitions, or a growth rate minimum. Nevertheless, self-poisoning is envisaged to affect crystal growth in the following manner. At any T_c there is a minimum fold length l_{min} below which attachments are more likely to melt than be built into the crystal. However, chain segments which are only slightly shorter than l_{min} will have a reasonably long lifetime as well as a higher attachment rate because of the lower barrier $F^* \propto l$. This would cause self-poisoning at any T_c. A snapshot of a cut normal to the surface of a growing crystal might thus look as in Figure 18. This situation corresponds to the "kinetic roughness" in the roughness-pinning model of Sadler.[23] With the exception of growth from dilute solution, the crystal growth surface for a polydisperse polymer would thus be covered most of the time by temporarily attached sections of chains which would block the progress of crystallization. Their removal would have to be included in the true entropic barrier

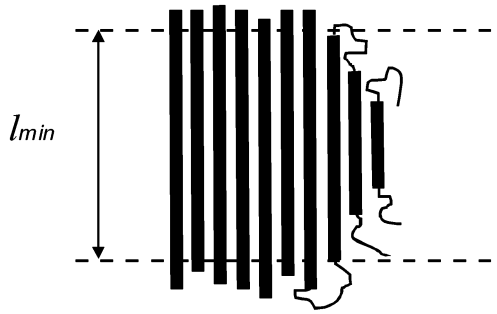

Figure 18. Snapshot of a typical section perpendicular to a self-poisoned crystal growth face as envisaged for a polydisperse polymer (also cf. ref 23).

for growth. This "pinning" contribution must therefore be added to that part of S^* which arises from the improbability of chain extension, expressed in different ways by Point[33] and Hoffman.[15]

The reason for self-poisoning in polyethylene being more pronounced at higher T_c, as suggested by morphology, remains one of a number of open questions.

Finally we note that, according to the above picture, crystallization of alkanes at small supercoolings presents an exceptional case of *low* self-poisoning, particularly in the case of shorter chains such as $C_{162}H_{326}$, where faceted untruncated lozenges form (Figure 14). This is because the only depositions having the potential to compete seriously with extended chains are once-folded chains. However, at small ΔT the dissolution temperature of the latter (T_d^F) is well below T_c, folded chains thus have a short lifetime and do not block the growth face. Unlike long alkanes, polyethylene never forms faceted crystals at temperatures above 100 °C; this is the case even at concentrations substantially lower than those employed in our alkane studies.[37,38] This adds credibility to the proposed idea of self-poisoning in polyethylene involving competing unstable depositions which have a reasonably long lifetime at any T_c. Thus, in long alkanes we see the self-poisoning effect at two extremes; it changes gradually from near zero at T_c sufficiently high above the growth transition temperature to extremely high at the rate minimum near the transition temperature. In contrast, except at very low concentrations and low T_c, self-poisoning is present in polyethylene under all circumstances. As expected, self-poisoning is reduced at low concentrations, resulting in faceted crystals.[6,39]

V. Conclusions

The following are the main conclusions of the present study.

(a) Self-poisoning is responsible for *curved growth faces* in long alkanes and is also a major factor in determining the G_{110}/G_{100} ratio, hence *determining the overall crystal habit*.

(b) Comparing the effects of self-poisoning on the two crystallographic faces, we find that G_{100} is *more retarded than* G_{110}.

(c) *Both the rates of initiation and propagation* (i_{100} *and* v_{100}) *pass through a minimum* at the extended to folded-chain growth transition. The significance of the minimum in v is that it can only be explained by assuming that the *barrier to step propagation is entropic*, rather than due to surface energy. Thus, while the discovery of self-poisoning has previously exposed the limitation of the coarse-grain treatment of secondary nucleation (deposition of complete stems), the present results reveal a similar inadequacy in dealing with the substrate completion process.

(d) Regarding i and v, it emerges that the *deposition of the first stem of a layer is impeded significantly more than the deposition of subsequent stems*.

(e) Comparison between long alkanes and polyethylene, regarding temperature dependencies of crystal habit, suggests that *self-poisoning also operates in polyethylene*, and *increasingly so at higher temperatures*.

(f) The binary phase diagram for $C_{246}H_{494}$−*n*-octacosane (solvent) exhibits classical behavior, reasonably well described by Flory−Huggins theory, with the metastable liquidus for once-folded crystals displaced by −10 K with respect to the equilibrium extended-chain liquidus.

Acknowledgment. The authors are indebted to Drs. G. M. Brooke, S. Burnett, and S. Mohammed for providing the long alkanes $C_{246}H_{494}$ and $C_{162}H_{326}$, and to Dr. X. B. Zeng for help in designing the T-jump stage. We acknowledge support from Engineering and Physical Science Research Council, the donors of the Petroleum Research Fund. administered by the American Chemical Society, and the University of Sheffield.

References and Notes

(1) Ungar, G.; Keller, A. *Polymer* **1987**, *28*, 1899.
(2) Organ, S. J.; Ungar, G.; Keller, A. *Macromolecules* **1989**, *22*, 1995.
(3) Ungar, G.; Zeng, X. B.; Brooke, G. M.; Mohammed, S. *Macromolecules* **1998**, *31*, 1875.
(4) Organ, S. J.; Keller, A.; Hikosaka, M.; Ungar, G. *Polymer* **1996**, *37*, 2517.
(5) Morgan, R. L.; Barham, P. J.; Hill, M. J.; Keller, A.; Organ, S. J. *J. Macromol. Sci.—Phys. B* **1998**, *37*, 319.
(6) Hobbs, J. K.; Hill, M. J.; Barham, P. J. *Polymer* **2001**, *42*, 2167.
(7) Ungar, G.; Mandal, P.; Higgs, P. G.; de Silva, D. S. M.; Boda, E.; Chen, C. M. *Phys. Rev. Lett.* **2000**, *85*, 4397.
(8) Higgs, P. G.; Ungar, G. *J. Chem. Phys.* **2001**, *114*, 6958.
(9) Higgs, P. G.; Ungar, G. *J. Chem. Phys.* **1994**, *100*, 640.
(10) Kovacs, A. J.; Gonthier, A.; Straupe, C. *J. Polym. Sci., Polym. Symp.* **1975**, *50*, 283.
(11) Putra, E. G. R.; Ungar, G. *Macromolecules* **2003**, *36*, 3812.
(12) Brooke, G. M.; Burnett, S.; Mohammed, S.; Proctor, D.; Whiting, M. C. *J. Chem. Soc., Perkin Trans. 1* **1996**, 1635.
(13) Flory, P. J. *J. Chem. Phys.* **1949**, *17*, 223. Mandelkern, L. *Crystallization of Polymers*; McGraw-Hill: New York, 1964; p 50.
(14) Hoffman, J. D. *Polym. Commun.* **1986**, *27*, 39.
(15) Hoffman, J. D.; Miller, R. L. *Polymer* **1997**, *38*, 3151.
(16) Ungar, G.; Stejny, J.; Keller, A.; Bidd, I.; Whiting, M. C. *Science* **1985**, *229*, 386.
(17) Hobbs, J. K.; Hill, M. J.; Keller, A.; Barham, P. J. *J. Polym. Sci. Part B: Polym. Phys.* **1999**, *37*, 3188.
(18) Toda, A. *Faraday Discuss.* **1993**, *95*, 129.
(19) Organ, S. J.; Keller, A.; Hikosaka, M.; Ungar, G. *Polymer* **1996**, *37*, 2517.
(20) Sutton, S. J.; Vaughan, A. S.; Bassett, D. C. *Polymer* **1996**, *37*, 5735.
(21) Mansfield, M. L. *Polymer* **1988**, *29*, 1755−1760.
(22) Cheng, S. Z. D.; Chen, J. H. *J. Polym. Sci., Part B: Polym. Phys.* **1991**, *29*, 311.
(23) Sadler, D. M. *Polymer* **1983**, *24*, 1401.
(24) Ungar, G.; Zeng, X. B. *Chem. Rev.* **2001**, *101*, 4157.
(25) Point, J. J.; Villers, D. *J. Cryst. Growth* **1991**, *114*, 228.
(26) Frank, F. C. *J. Cryst. Growth* **1974**, *22*, 233.
(27) Hoffman, J. D.; Miller, R. L. *Macromolecules* **1989**, *22*, 3038, 3502. Hoffman, J. D.; Miller, R. L. *Polymer* **1991**, *32*, 963.
(28) Toda, A. *J. Phys. Soc. Jpn.* **1986**, *55*, 3419.
(29) Ungar, G.; Putra, E. G. R. *Mcromolecules* **2001**, *34*, 5180.

(30) Hoffman, J. D.; Weeks, J. J. *J. Chem. Phys.* **1965**, *42*, 4301.
(31) de Silva, D. S. M.; Ungar, G. Manuscript in preparation.
(32) Lauritzen, J. I. *J. Appl. Phys.* **1973**, *44*, 4353.
(33) Point, J. J. *Macromolecules* **1979**, *12*, 770. Point, J. J. *Discuss. Faraday Soc.* **1979**, *68*, 167.
(34) Sadler, D. M. *Nature (London)* **1987**, *326*, 174.
(35) Welch, P.; Muthukumar, M. *Phys. Rev. Lett.* **2001**, *87*, 218302.
(36) Toda, A.; Arita, T.; Hikosaka, M. *Polymer* **2001**, *42*, 2223.
(37) Organ, S. J.; Keller, A. *J. Mater. Sci.* **1985**, *20*, 1571.
(38) Khoury, F. *Faraday Discuss., Chem. Soc.* **1979**, *68*, 404.
(39) Organ, S. J.; Ungar, G.; Keller, A. *J. Polym. Sci., Part B: Polym. Phys. Ed.* **1990**, *28*, 2365.

MA034074H